Environmental Science Advances

ROYAL SOCIETY OF CHEMISTRY

PAPER

View Article Online
View Journal | View Issue

Cite this: *Environ. Sci.: Adv.*, 2025, **4**, 2154

Amine-functionalised monolithic silica adsorbents for CO_2 capture

Ali Kasiri,[a] R. Sanz,[bc] Eloy S. Sanz-Pérez[a] and Amaya Arencibia *[a]

Received 15th August 2025
Accepted 20th October 2025

DOI: 10.1039/d5va00269a

rsc.li/esadvances

This study explored the CO_2 adsorption properties of amine-functionalised siliceous monoliths with enhanced efficiency for CO_2 capture. Silica cylindrical monolithic macroscopic structures were successfully prepared from the polymerization of the silica source (TEOS) condensed on surfactant Pluronic P-123 or F-127, and using acrylamide. Previously synthesized SBA-15 was also used to prepare the monolithic structure. Materials were functionalised by grafting with two aminosilanes, 3-(trimethoxysilyl)propylamine (AP) and N^1-(3-trimethoxysilylpropyl)diethylenetriamine (DT). A positive correlation was found between the amount of amines grafted and the total CO_2 uptake under pure and dry conditions. Nevertheless, the efficiency of amines (mol of CO_2 per mol of N) was lower for highly loaded samples due to reduced site accessibility. DT functionalization of the monoliths was found to produce the best results within the concentrations studied, surpassing AP-functionalized monoliths, with P-123 monolith-2DT reaching a CO_2 uptake as high as 108 mg g^{-1} at 1 bar and 156 mg g^{-1} at 5.5 bar (both at 45 °C). They also achieved CO_2 uptakes at 0.15 bar which were 54–87% of the values in pure CO_2, indicating the obtention of highly selective sorbents. Moreover, aminated monoliths also showed stable uptakes over 5 adsorption–desorption cycles and over 20 cycles in the case of P-123 monolith-2DT, where it maintained 79% of its initial capacity under pure CO_2 and 85% of it under 15% CO_2.

Environmental significance

Low-pressure-drop adsorbents such as monoliths are essential to translate laboratory sorbent performance into industrial CO_2-capture devices, as they mitigate clogging associated with excessive pressure drop in powdered materials. Here, silica monoliths were covalently grafted with amine-containing aminopropyl (AP) and diethylenetriamine (DT) moieties, and their CO_2 adsorption properties were evaluated at 45 °C and 1 bar. A trade-off was found for these monoliths, since increasing nitrogen content raises capacity but diminishes amine efficiency, establishing practical loading windows for monoliths. Under dilute conditions similar to flue gas (0.15 bar CO_2), the adsorbents achieved 54–87% of the uptake measured in pure CO_2, indicating a highly selective process that could be applied under such conditions, thus increasing the applicability of CO_2 capture technology.

1 Introduction

Anthropogenic CO_2 emissions from energy and industry are the primary driver of the observed global warming. The achievement of the Paris Agreement of 2015 for temperature (<2 °C, ideally 1.5 °C) requires deep emission cuts across sectors, including capture at large point sources. Carbon capture and storage (CCS) complements renewables and efficiency by removing CO_2 from hard-to-abate facilities for permanent storage or use.[1,2]

Adsorption-based carbon capture has garnered substantial interest as a viable mitigation strategy due to its high operational efficiency and seamless integration with existing industrial infrastructure.[3,4] This technique entails the retention of CO_2 molecules on the surface of solid adsorbents through either physisorption or chemisorption mechanisms. The performance of the adsorption process is highly dependent on the intrinsic properties of the adsorbent, including its surface area, pore size distribution, and surface chemical functionality.[5,6] Extensive research has been directed toward the development of advanced adsorbent materials that optimize CO_2 capture performance.[7–9] Among these materials, activated carbons, zeolites, clays, metal–organic frameworks (MOFs), and particularly mesostructured silica and alumina have demonstrated considerable adsorption performance for CO_2 capture.[6] MOF materials have shown very significant CO_2 adsorption capacities at high pressure due to specific metallic adsorption sites and the small micropore channels.[10] Thus, in the literature it can be found that high-surface-area physisorbents such as MOF-177 reach

[a]*Department of Chemical, Energy, and Mechanical Technology, ESCET, Universidad Rey Juan Carlos, C/Tulipán s/n, 28933 Móstoles, Madrid, Spain. E-mail: amaya.arencibia@urjc.es*

[b]*Department of Chemical and Environmental Technology, ESCET, Universidad Rey Juan Carlos, C/Tulipán s/n, 28933 Móstoles, Madrid, Spain*

[c]*Instituto de Investigación de Tecnologías para la Sostenibilidad, Universidad Rey Juan Carlos, C/Tulipán s/n, 28933 Móstoles, Madrid, Spain*

~33.5 mmol of CO_2 per g at 35 bar and 25 °C but only ~0.8 mmol g^{-1} at 1 bar, whereas open-metal-site chemisorbents like Mg-MOF-74 achieve ~9–10 mmol of CO_2 per g at 1 bar (25 °C).[11] MOF materials stand out when pore polarity and open sites are optimised for the target pressure window, while amine-functionalized mesoporous silicas, either by grafting and impregnation, provide tuneable chemisorption at flue-gas-relevant temperatures at atmospheric pressure with high capacities (higher than 5 mmol of CO_2 per g) and regeneration possibility. Mesostructured materials displayed good behaviour as adsorbents due to their high surface areas and tunable mesoporous architectures, which enable enhanced adsorption capacity and selectivity for CO_2 molecules. Mesostructured silica and alumina, synthesized *via* sol–gel methodologies employing structure-directing agents, allow precise tailoring of pore size, volume, and surface area, thereby facilitating targeted application-specific performance.[12,13]

Porous materials can be further optimized through surface functionalisation with amine groups, a strategy that enhances their CO_2 adsorption *via* chemisorption. Comprehensive reviews have summarized the progress in amine-functionalised silica adsorbents over the past five years, discussing synthesis methods, factors affecting adsorption performance, and future research directions.[14] These advancements underscore the importance of tailored functionalisation strategies and the utilisation of sustainable materials to enhance the efficiency and applicability of mesoporous silica in CO_2 capture technologies. This functionalisation typically involves covalent grafting of amine moieties onto the adsorbent surface. The resulting amine-functionalised materials exhibit improved CO_2 uptake through the formation of stable carbamate species, which significantly enhances adsorption capacity with respect to physisorption. Their distinct physicochemical properties, such as their thermal robustness or the ability of covalently bonded amines to withstand cyclic processes, make them highly suitable candidates for deployment in industrial operational environments.[15–18]

These investigations collectively highlight that the selection of aminosilane type, loading amount, and surface engineering – such as silanol activation or co-grafting techniques – can drastically influence both the CO_2 adsorption capacity and the operational resilience of silica-based adsorbents. The density of accessible amine groups, and consequently the CO_2 uptake, is significantly influenced by the surface hydroxyl density of the silica, which can be enhanced through mild template removal methods like ethanol extraction as opposed to high-temperature calcination.[19] Studies have shown that higher silanol densities lead to increased grafting efficiency and stronger CO_2 interactions, evidenced by the formation of ionic and surface-bound carbamates detectable *via* FTIR spectroscopy. Additionally, the spatial arrangement of amine groups – controlled through steric hindrance or co-grafting strategies – plays a critical role in determining the stability and capacity of the adsorbents during repeated cycles. These findings underscore the importance of optimizing both the textural and chemical surface properties of mesoporous supports to maximise the effectiveness of CO_2 adsorption *via* amine grafting. As a result, amine-functionalised mesostructured silica remains a benchmark material in the development of solid adsorbents for post-combustion carbon capture applications.

As functionalisation techniques evolve, emphasis is increasingly placed on balancing adsorption performance with long-term structural integrity, scalability, and environmental sustainability. Recent advancements in amine-functionalised mesoporous silica materials have shown significantly enhanced CO_2 capture performance. For instance, SBA-15 functionalised with 3-aminopropyltriethoxysilane (APTES) and L-lysine exhibited a CO_2 adsorption capacity of 4.53 mmol of CO_2 per g at 2 bar and room temperature, demonstrating the synergistic effect of dual amine functionalities.[20] Similarly, a study on amine-functionalised mesoporous silica derived from natural sources reported improved CO_2 adsorption capacities, highlighting the potential of sustainable materials in carbon capture applications.[21] Furthermore, research into the optimization of surface silanol groups in SBA-15 and KIT-6 materials revealed that increasing the number of these groups facilitates better APTES functionalisation, leading to increased CO_2 adsorption capacities and improved material stability over multiple cycles.[22]

Despite the promising performance of powder adsorbents under controlled laboratory conditions, their widespread implementation in industrial environments faces several limitations. These include handling challenges such as particle agglomeration, greater pressure drop during gas flow through packed beds, and material attrition during repetitive adsorption–desorption cycles. Such issues undermine process efficiency and complicate large-scale deployment. Consequently, the focus has progressively shifted toward the development of agglomerates, extruded or similar arrangements. Among them, monolithic adsorbents are a robust alternative, offering several intrinsic advantages over powder-based systems. Their organized geometry ensures a lower pressure drop, superior flow distribution, and improved mechanical integrity under operational stress, well-suited for continuous practical application. Moreover, these structures can be tailored to possess high surface areas and hierarchically organized porosity, needed for efficient CO_2 uptake.[23,24]

The incorporation of amine functionalities into monolithic frameworks has been a pivotal step in improving their affinity toward CO_2. Strategic placement of aminosilanes within the monolith matrix allows for stronger interactions between the adsorbent and CO_2 molecules, thereby enhancing both capacity and selectivity.[8]

In recent years, significant advancements have been made in the fabrication of monolithic adsorbents tailored for CO_2 capture, particularly through the application of 3D printing technologies. Rezaei *et al.* formulated aminosilica-based monoliths using a robocasting technique, successfully incorporating tetraethylenepentamine (TEPA), poly(ethylenimine) (PEI), and 3-aminopropyltrimethoxysilane (APS) into the silica matrix while maintaining structural integrity and comparable performance to powdered analogues.[23] In a related study, they demonstrated the viability of 3D-printed MOF monoliths using MOF-74(Ni) and UTSA-16(Co), showing that high adsorbent

loadings (≥80 wt%) could be achieved without compromising mechanical strength or adsorption efficiency. These works underscore the importance of shaping techniques in transforming high-performance powdered adsorbents into scalable, low-pressure-drop structures suited for industrial-scale applications.[24]

Collectively, these studies demonstrate that combining advanced manufacturing techniques with targeted chemical functionalisation enables the development of structurally stable and high-performance monolithic adsorbents, thus addressing the operational limitations of conventional powder-based materials in CO_2 capture systems.[25] In another study, the fabrication of 3D-printed self-standing zeolite monoliths using 13X and 5A zeolite powders was introduced, targeting efficient CO_2 removal from enclosed environments such as spacecraft and submarines.[26] These monoliths were engineered through a robocasting technique and exhibited hierarchical pore networks with improved mechanical strength and structural integrity compared to conventional pellet-based systems.

Other advancements have introduced the synthesis of hierarchically porous silica monoliths by integrating sol–gel chemistry with phase separation techniques. This synthesis strategy allows the formation of interconnected macro- and mesoporous networks, offering multiscale control over porosity while maintaining structural integrity. Such hierarchical designs not only streamline the fabrication process but also improve mass transfer characteristics within the monoliths, which is critical for achieving high-performance gas adsorption.[26]

Despite the increased interest in amine-functionalised mesoporous materials, few studies have systematically compared the performance of monolithic silica adsorbents functionalised with different aminosilanes under identical synthesis and testing conditions. Some recent works have demonstrated the potential of monolithic structures to overcome limitations of powdered adsorbents, such as pressure drop and mechanical fragility. In this work, the preparation of monolithic macroporous structures based on amino-functionalised mesostructured silica has been studied. This study addresses the evaluation of the CO_2 adsorption performance, structural stability, and efficiency of aminopropyl (AP) and diethylenetriamine (DT)-functionalised monoliths based on SBA-15, and direct condensed silicas polymerized on Pluronic P-123 and F-127 templates.

2 Experimental section

2.1 Reagents and materials

N,*N*′-Methylenebisacrylamide (MBA, $C_7H_{10}N_2O_2$, 99%) and acrylamide (AM, C_3H_5NO) were employed as the primary monomers in the formulation of the polymer matrix, both procured from Sigma-Aldrich. Ammonium persulfate (APS, $(NH_4)_2S_2O_8$, 98%) served as the free-radical initiator to trigger polymerization, with methanol and ethanol utilised as solvents to facilitate the reaction. Tetraethyl orthosilicate (TEOS, reagent grade, 98%) was used as the silica precursor for constructing the inorganic framework, while furfuryl alcohol (FA, synthesis grade) was incorporated as a pore-forming agent. Pluronic F-127 and Pluronic P-123 block copolymers, acting as structure-directing agents for mesopore formation, were also sourced from Sigma-Aldrich. The hydrolysis and condensation steps essential for monolith synthesis were catalysed by hydrochloric acid (HCl, 37%) supplied by Scharlab.

In this study, SBA-15 mesostructured silica was used as the foundational material for fabricating SBA-15-based monoliths, following a synthesis protocol adapted from the method reported by Zhao *et al.*[27] Tetraethyl orthosilicate (TEOS) served as the silica precursor, while Pluronic P123 was employed as the structure-directing agent to guide the formation of the mesoporous framework. The synthesis began with the dissolution of 72 g Pluronic P123 in an aqueous hydrochloric acid solution (2.7 L, 1.9 M HCl), after which 155.8 g TEOS was gradually added under continuous stirring. The mixture was then maintained at 40 °C for 20 hours to facilitate hydrolysis, followed by an aging process at 110 °C for 24 hours to promote structural development. The resulting solid product was recovered *via* filtration, subsequently dried, and calcined under air using a ramp rate of 1.8 °C min^{-1} to 550 °C followed by a 5 h isothermal hold, to remove the organic template, yielding highly ordered SBA-15 mesoporous silica.

2.2 Fabrication of monolithic adsorbents

This study explores the potential of silica-based monolithic materials as adsorbents for CO_2 capture, focusing on two primary synthesis strategies: (i) monoliths derived from pre-synthesized SBA-15 mesostructured silica, and (ii) direct synthesis of monoliths employing Pluronic P-123 and Pluronic F-127 as structure-directing agents. The initial development phase emphasized optimizing key structural features, such as porosity and surface area, to establish a suitable framework for subsequent functionalisation aimed at enhancing CO_2 adsorption performance.

The fabrication of SBA-15-based monoliths was adapted from protocols previously applied to MCM-41-type materials.[28] The process began with the preparation of a homogeneous aqueous solution of acrylamide (AM, 1.5 g), *N*,*N*′-methylenebisacrylamide (MBA, 0.15 g), and ammonium persulfate (APS, 0.015 g) in 30 mL deionized water, stirred to clarity. SBA-15 powder (1.5 g) was dispersed under vigorous stirring (2 h, RT) to ensure uniform distribution. The resulting mixture was then centrifuged at 5000 rpm for 5 min, transferred to cylindrical moulds ($Ø \times L = 2$ cm × 8 cm), and polymerized at 60 °C for 12 h to form monolith hydrogels. After demoulding, samples were dried and calcined at 550 °C for 10 h to remove organics and obtain the mesostructure.

For the direct synthesis of silica monoliths, Pluronic P-123 and F-127 were employed as soft templates to guide the formation of ordered mesoporous frameworks. This method, previously reported in the literature,[26] aimed to exploit the templating ability of these non-ionic surfactants to achieve materials with high surface areas and large pore volumes, which are crucial for efficient CO_2 adsorption. The synthesis involved the formation of a silica sol by refluxing tetraethyl

orthosilicate (TEOS) in ethanol and 0.14 M hydrochloric acid. The solution was subsequently cooled and stored at 4 °C until further use.

Pre-hydrolysed TEOS sol was prepared by refluxing TEOS (10.5 g)/EtOH (6.9 g)/0.14 M HCl (0.9 g) for 2 h and stored at 4 °C. A surfactant solution consisting of 2.5 g Pluronic F-127 or P-123 in 5 g 0.12 M HCl was combined with the TEOS sol and 13.6 g furfuryl alcohol (FA) and mixed for 2 min. Under acidic conditions, FA undergoes cationic polymerization into poly(-furfuryl alcohol) (PFA), initiating phase separation due to the increasing hydrophobicity of PFA. This polymerization-induced phase separation mechanism leads to the development of an interconnected macroporous network, where the polymeric domains serve as templates for the macropores, while the surrounding silica undergoes sol–gel transition to form the structural matrix. The resulting mixture was left to age at room temperature for 48 to 72 h to facilitate solvent evaporation and promote structural organization.

The gelled materials were then cast into cylindrical moulds ($Ø \times L = 20$ mm $\times$ 20 mm) and thermally treated in a stepwise manner. The initial curing was performed at 65 °C for 72 h to promote gradual condensation, followed by a second curing stage at 135 °C for an additional 48 h to complete polymerization and structural consolidation. The monoliths were finally subjected to calcination under a controlled airflow. The temperature ramp for calcination involved a multi-stage heating profile: an initial ramp of 10 °C min^{-1} to 130 °C, followed by 2 °C min^{-1} to 450 °C, and a final ramp of 1 °C min^{-1} up to 550 °C. This gradual heating strategy ensured the complete removal of organic templates while preserving the structural integrity of the silica framework.

2.3 Synthesis of amino-functionalised monoliths

A solvothermal grafting technique in a toluene medium was employed to functionalise the silica monoliths, leveraging the monolith framework as a stable scaffold for surface chemisorption. In this process, the monolith was initially dispersed in a round-bottom flask with toluene (250 mL toluene per gram of silica), after which selected organosilanes, 3-(trimethoxysilyl) propylamine (AP) and *N*-(3-trimethoxysilylpropyl)diethylenetriamine (DT), were introduced. An amount of silane of 6.92 mmol per g silica was used, corresponding to 1.24 g AP per g silica and 1.83 g DT per g silica. Considering the specific surface areas of the synthesised monoliths, 833 $m^2 g^{-1}$ for SBA-15 monolith, 435 $m^2 g^{-1}$ for P-123 monolith, and 378 $m^2 g^{-1}$ for F-127 monolith; (see the Results and discussion section) and that silica calcined at 550 °C has a surface concentration of 1.7 SiOH per nm^2,[29,30] the samples exhibit SiOH concentrations of 2.35, 1.23, and 1.07 mmol g^{-1} for SBA-15, P-123, and F-127 monoliths, respectively. When adding a constant 6.92 mmol of silane per gram of silica, the resulting silane : surface SiOH molar ratios are 2.9, 5.6, and 6.5 for SBA-15, P-123, and F-127 monoliths, ensuring a sufficient excess of silanes in the grafting reaction. The functionalisation reaction was carried out under reflux conditions for 24 h to ensure effective covalent bonding between the silane molecules and the monolith surface. To investigate the influence of functional group density on CO_2 adsorption performance, the grafting was also conducted using double the molar amount of each aminosilane (13.84 mmol of silane per gram of silica, yielding 2AP and 2DT samples), thereby enhancing the concentration of reactive nitrogen-containing sites.

Post-grafting materials were subjected to a purification step involving vacuum filtration to remove any unreacted or weakly adsorbed silane species, ensuring chemical purity and structural consistency. The monoliths were then air-dried under ambient conditions. This mild drying approach was chosen to preserve the chemical integrity of the grafted amine functionalities, which could otherwise be compromised by high-temperature treatments, potentially diminishing their CO_2 capture efficiency.

The synthesized materials were systematically labelled using the nomenclature Z-monolith-*X*Y, where 'Z' denotes the specific type of base monolith employed, namely P-123, F-127, or SBA-15. The variable '*X*' corresponds to the amount of the aminosilane reagent used, while 'Y' denotes the type of organosilane functional group applied (*e.g.*, AP or DT).

2.4 Characterization

The synthesized adsorbents underwent comprehensive physicochemical characterization to evaluate their suitability for CO_2 capture. Chemical composition was assessed *via* elemental microanalysis to determine nitrogen content, using a CHNOS analyser (Flash 2000, Thermo Fisher Scientific). Textural properties were analysed by studying nitrogen adsorption–desorption isotherms measured at 77 K using a Micromeritics Tristar 3000 sorptometer. Prior to measurements, samples were degassed in N_2 flux at 200 °C for 480 min (non-functionalised monoliths) or at 150 °C for 480 min (amine containing samples). The specific surface area was calculated using the Brunauer–Emmett–Teller (BET) method within the relative pressure range of 0.05–0.30, while pore size distribution was derived from the adsorption branch of the isotherms using the Barrett–Joyner–Halenda (BJH) model.[31]

Structural ordering and mesostructure of the synthesized materials were investigated *via* low angle X-ray diffraction (XRD) using a PANalytical Empyrean powder diffractometer configured in a θ/θ geometry. The instrument was equipped with a Wonder ultrafast detector, an Anton Paar XRK 900 high-temperature chamber, and a diffracted beam optics system suitable for parallel beam (thin film) analysis (Cu Kα radiation; 0.53–5.0° scanning low range of the diffraction angle 2θ; step 0.03°; 5 s per step), with optic selection focusing on low-angle XRD, typically used for characterizing mesoporous materials, where large periodicities produce reflections at low angles. These measurements enabled the detection of variations in mesostructural order arising from different synthesis routes and post-synthetic functionalisation processes, providing critical insight into the structural integrity and periodicity of the mesoporous frameworks.

To assess the CO_2 adsorption behaviour under dynamic conditions, thermogravimetric analysis (TGA) was conducted

using a METTLER Toledo TGA/SDT system, capable of operating at temperatures up to 1600 °C. Each sample (10–20 mg, taken as bulk cuts from the original monoliths) was first degassed at 110 °C for 2 hours under a nitrogen flow (100 mL min^{-1}) until the mass-loss plateau was reached to eliminate residual surface adsorbates. CO_2 adsorption was then monitored over a 3 hour period under a continuous CO_2 flow (100 mL min^{-1}). Measurements were performed at 45 °C to simulate post-combustion CO_2 capture conditions relevant to flue gas treatment.

Additionally, equilibrium CO_2 adsorption–desorption isotherms were recorded using a high-pressure volumetric analyser (HPVA-100, VTI Scientific Instruments) within a pressure range of 0–6 bar at 45 °C. Prior to measurements, approximately 150 mg of sample was loaded into the analysis cell and outgassed at 110 °C for 2 h under high vacuum ($4–8 \times 10^{-3}$ mbar). Helium void-volume corrections were determined at 45 °C over 1–6 bar. During CO_2 adsorption at 45 °C, each isotherm point was acquired when the residual pressure change was below 0.2 mbar over 3 min; if unmet, a maximum equilibration time of 50 min was applied. The sample cell temperature was controlled at 45 °C using a thermostatic external bath. This multi-technique approach provides a robust framework for evaluating the adsorption capacity, kinetics, and structural stability of the developed monolithic adsorbents.

CO_2 uptake, q (mg CO_2 per g) and CHN nitrogen content (wt%) were each converted to moles per gram to calculate the amine efficiency as the ratio of moles of CO_2 adsorbed to moles of nitrogen (mol of CO_2 per mol of N). Uncertainties were estimated by first-order propagation from independent absolute uncertainties of ±2 mg g^{-1} for uptake and ±0.10 wt% for nitrogen, which gives uncertainty values of 0.01–0.03 mol of CO_2 per mol of N across all samples.

3 Results and discussion

The monolithic porous macrostructures obtained in this work are shown in Fig. 1, where samples display colour changes reflecting different steps of the synthesis. The initial monolith appears black prior to calcination (a), representing the as-synthesized material containing organic residues. After calcination, the monolith changes to white (b), indicating the successful removal of organic templates and the development of a porous inorganic network. Finally, the yellow coloration denotes the post-functionalisation stage (c), where aminosilane groups have been successfully grafted onto the silica surface, tailoring the monolith for enhanced CO_2 adsorption performance.

3.1 Characterization of non-functionalised adsorbents (silica monoliths)

The structural analysis of the synthesized monolithic adsorbents (P-123 monolith, F-127 monolith, and SBA-15 monolith), along with SBA-15 powder, was conducted using X-ray diffraction (XRD) to evaluate the mesostructural ordering. As shown in Fig. 2, the XRD pattern of SBA-15 powder displayed sharp and well-resolved reflections corresponding to the (100), (110), and (200) planes, characteristic of a highly ordered two-dimensional hexagonal mesoporous structure (space group *P6mm*).[27,28]

The SBA-15 monolith exhibited similar peak positions but with reduced intensity and broader features, indicating partial disruption of long-range order while preserving the overall mesoporous framework. This reduction in mesostructured order may result from structural alterations during monolith formation, potentially associated with the use of polymeric binders or additives that influence the assembly of the silica network during the sol–gel and aging processes.[32]

For the P-123 and F-127 monoliths, XRD patterns exhibited no discernible diffraction peaks in the low-angle region, suggesting a further reduction in structural order compared to SBA-15-based materials, likely due to differences in synthesis conditions and the use of Pluronic P-123 and F-127 as structure-directing agents. These results indicate that although mesoporosity is present, the degree of uniformity and mesophase

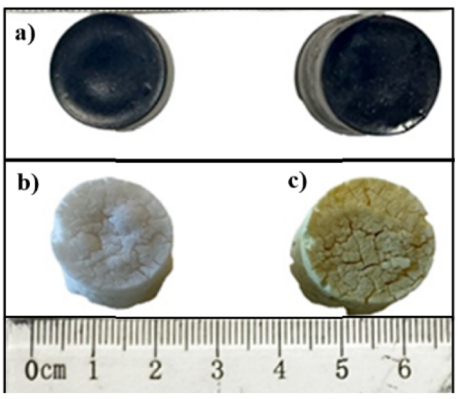

Fig. 1 Prepared silica monoliths: (a) non-calcined, (b) calcined, and (c) functionalised.

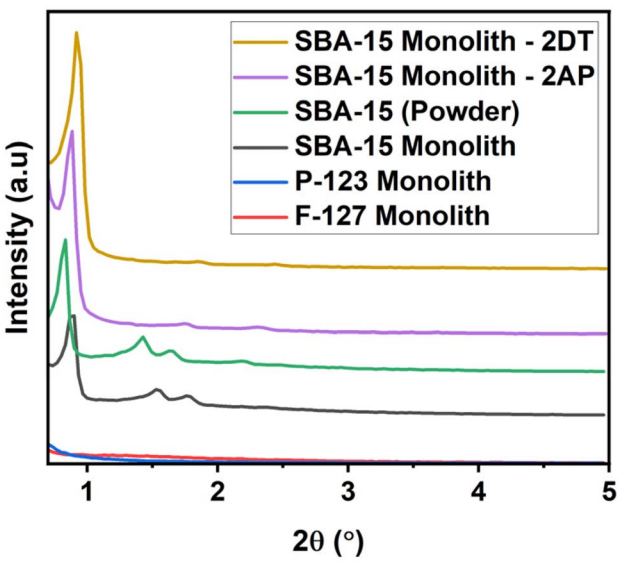

Fig. 2 Powder low angle X-ray diffraction patterns of pure pre-synthesized SBA-15 powder and monolithic adsorbents.

organization in the P-123 and F-127 monoliths is significantly lower than that of SBA-15 powder and SBA-15 monolith, reflecting the influence of synthesis strategy on the resulting framework structure. These observations align with previous studies where the use of Pluronic surfactants under certain synthesis conditions led to reduced mesostructural ordering. For instance, Zhao and Shi[27,33] reported that variations in synthesis parameters, such as temperature and surfactant concentration, significantly impact the structural order of mesoporous silica materials synthesized with Pluronic P123 and F127. Additionally, studies have shown that the incorporation of additives or modifications in the synthesis process can further influence the degree of mesostructural ordering in these materials.[34]

The nitrogen adsorption–desorption isotherms offer valuable insights into the textural characteristics of the synthesized adsorbents (Fig. 3a). SBA-15 powder displayed a typical type IV isotherm with a well-defined H1 hysteresis loop, consistent with the presence of uniform mesoporous structures. The sharp increase in nitrogen uptake at high relative pressures further confirms the existence of large and uniform mesopores. In contrast, the SBA-15 monolith, while retaining mesoporosity, exhibits an H3 hysteresis loop, indicating the coexistence of meso- and macropores and suggesting a more heterogeneous pore structure compared to the powder form.

The isotherms for P-123 and F-127 monoliths also conform to type IV classification; however, they present less pronounced hysteresis loops and a more gradual adsorption profile. These characteristics imply the presence of more irregular and diverse pore structures, potentially due to synthesis-induced variations or structural imperfections.

The pore size distribution curves (Fig. 3b) further differentiate these materials. SBA-15 powder features a narrow distribution centred around 9.2 nm, characteristic of a highly ordered mesoporous network. Conversely, the monoliths exhibit broader and less defined distributions, indicative of greater heterogeneity in pore size and suggesting a more amorphous or disordered porous framework.

Table 1 summarizes the main textural properties of these materials in terms of surface area and pore volume, SBA-15 powder exhibits the highest BET value at 861 $m^2\ g^{-1}$ and pore volume (1.55 $cm^3\ g^{-1}$), followed closely by SBA-15 monolith at 833 $m^2\ g^{-1}$ with a pore volume of 1.30 $cm^3\ g^{-1}$. In contrast, P-123 and F-127 monoliths present significantly lower surface areas of 435 $m^2\ g^{-1}$ and 378 $m^2\ g^{-1}$, and pore volumes of 0.86 $cm^3\ g^{-1}$ and 0.75 $cm^3\ g^{-1}$, respectively. These disparities are primarily attributed to differences in synthesis methodology, where the direct formation of monolithic structures may lead to reduced porosity and potential pore collapse, resulting in lower accessible surface areas.

Fig. 4 displays the CO_2 adsorption capacities of the synthesized monoliths and SBA-15 powder at 45 °C and 1 bar. The adsorption order is as follows: SBA-15 powder (27 mg CO_2 per g) > SBA-15 monolith (14 mg CO_2 per g) > P-123 monolith (11 mg CO_2 per g) > F-127 monolith (6 mg CO_2 per g). While these values are modest, they reveal discernible differences attributable to the structural and surface characteristics of the materials. Fig. 3a, b and Table 1 provide insights into the textural parameters influencing CO_2 uptake. Although SBA-15 monolith

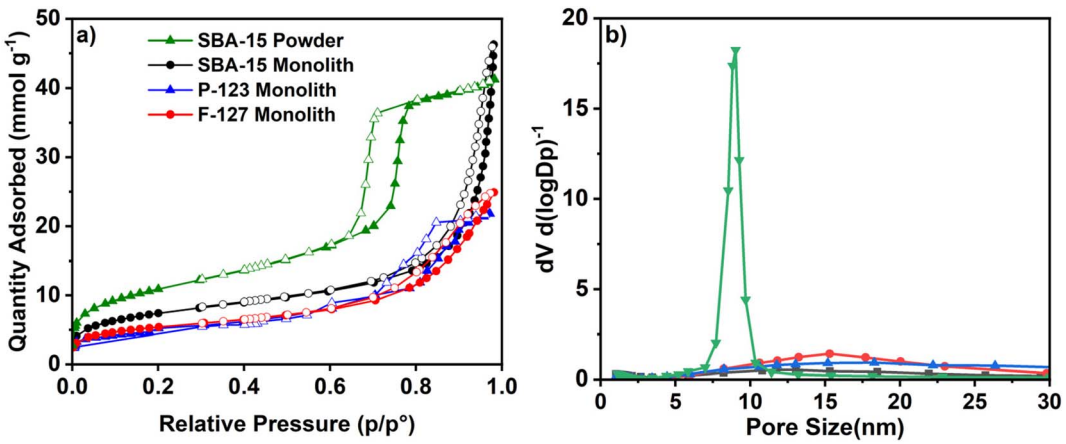

Fig. 3 (a) N_2 adsorption–desorption isotherms at 77 K, and (b) pore size distribution of all monoliths and SBA-15 powder.

Table 1 Textural properties and CO_2 adsorbed amount of monoliths and SBA-15 powder

Sample	S_{BET} ($m^2\ g^{-1}$)	V_p ($cm^3\ g^{-1}$)	D_p (nm)	q^a (mg CO_2 per g)
SBA-15 powder	861	1.55	9.2	27
SBA-15 monolith	833	1.30	—	14
P-123 monolith	435	0.86	—	11
F-127 monolith	378	0.75	—	6

[a] CO_2 adsorption capacity (mg CO_2 per g) was measured using thermogravimetric analysis (TGA) under pure CO_2 at 45 °C and 1 bar.

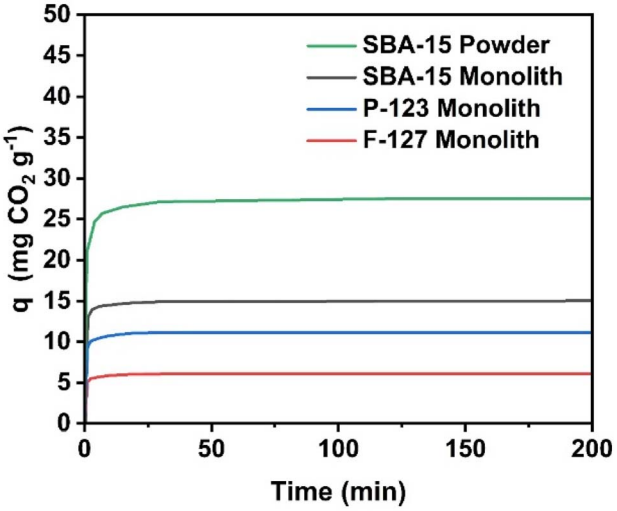

Fig. 4 Pure CO_2 uptake (45 °C, 1 bar) of silica monoliths and SBA-15 powder.

and powder show similar surface areas (~833 and 861 $m^2\ g^{-1}$, respectively), the powder achieves nearly double the CO_2 adsorption, likely due to its highly ordered and accessible mesoporous network. The comparatively lower CO_2 uptakes observed in the P-123 and F-127 monoliths (11 mg CO_2 per g and 6 mg CO_2 per g, respectively) are consistent with their reduced BET surface areas (435 and 378 $m^2\ g^{-1}$) and pore volumes (0.86 and 0.75 $cm^3\ g^{-1}$), highlighting the relevance of textural properties.

Nevertheless, the CO_2 uptake remains limited in all cases, and further surface modification would be necessary to achieve practical capture capacities.

These findings align with previous studies on gel-cast MCM-41 monoliths, which also demonstrated hierarchical porosity comprising both meso- and macropores, thereby enhancing accessibility and diffusion pathways for adsorbates.[35] Additionally, the use of Pluronic F-127 as a structure-directing agent has been shown to significantly affect the final pore architecture. In this work, the F-127-based monoliths displayed lower textural properties than their SBA-15 counterparts, a trend consistent with literature reports indicating that increased F-127 concentrations promote macropore formation and enhanced mass transport, albeit at the expense of mesopore regularity and surface area.[26]

3.2 Characterization of amino functionalised monoliths

Fig. 2 shows the X-ray diffraction (XRD) patterns of SBA-15-based monoliths before and after surface functionalisation with aminosilanes. Samples exhibit reflections characteristic of ordered mesoporous structures, although the (110) and (200) reflections appeared less distinct after functionalisation, indicating a reduction in long-range order and an increase in structural disorder across higher-order planes. This is consistent with observations in previously studied amine-modified SBA-15 materials[32] often attributed to partial pore blockage or reduced structural ordering. Nevertheless, the mesoscopic order features remain identifiable, indicating that the functionalisation process did not significantly disrupt the underlying framework.

In addition to the intensity changes, a slight shift in the diffraction peak positions toward higher 2θ angles was observed in the functionalised SBA-15 samples. This shift suggests a reduction in the unit cell parameter, which is commonly attributed to pore contraction or thickening of the pore walls due to the incorporation of organosilane moieties during grafting. Similar structural changes have been reported in functionalised mesoporous silicas, where post-synthetic modification alters the mesostructural dimensions.[36,37]

Complementary to XRD analysis, nitrogen adsorption–desorption isotherms were used to evaluate the influence of functionalisation on the porosity of monoliths derived from P-123, F-127, and SBA-15 templates. As shown in Fig. 5, functionalised monoliths showed a reduced nitrogen uptake compared to their non-functionalised counterparts. Nevertheless, they retained, in general, type IV isotherms with well-defined hysteresis loops, indicating the preservation of mesoporous features. This trend was more marked when using a longer functionalising agent (DT moieties) or a larger organic amount (2AP and 2DT), as previously reported.[15,38] The resulting mesoporosity of the functionalised samples was, as expected, dependent on the textural properties of the parent monolith. This way, SBA-15 monolith, with the largest textural properties, yielded modified materials with the largest pore structures. This was followed by functionalised versions of P-123 monolith and, finally, F-127 monolith. In the more significant cases, DT-functionalised F-127 monoliths, especially at higher loadings (2DT), demonstrated a marked reduction in nitrogen uptake and a near-complete disappearance of hysteresis loops, suggesting extensive pore filling with organic compounds.

Quantitative textural data further confirm these observations. The pristine P-123, F-127 and SBA-15 monoliths exhibit classic type-IV isotherms with H1/H2 hysteresis, indicative of well-ordered mesoporosity. After AP grafting, the type-IV profile and capillary loop remain largely intact (Fig. 5a and b), mirroring the behaviour of APTES-grafted hierarchically porous silica previously reported.[39]

Quantitative data shown in Table 2 corroborate these trends. SBA-15 proves most resilient: 1AP retains 336 $m^2\ g^{-1}$/1.05 $cm^3\ g^{-1}$ (15.1 nm), 2AP still offers 199 $m^2\ g^{-1}$/0.55 $cm^3\ g^{-1}$ (11.5 nm), and even 2DT preserves 65 $m^2\ g^{-1}$/0.11 $cm^3\ g^{-1}$ with a discernible 6 nm peak, outperforming the triamine-grafted alumina honeycomb described by Grossmann *et al.*[40] (Fig. 5a and b).

For P-123, the functionalisation with 1AP lowered the BET surface area and total pore volume from 435 $m^3\ g^{-1}$ and 0.86 $cm^3\ g^{-1}$ to 260 $m^2\ g^{-1}$ and 0.50 $cm^3\ g^{-1}$, respectively, while the use of 2AP pushed them to 149 $m^2\ g^{-1}$ and 0.28 $cm^3\ g^{-1}$, with a modest pore-size shift to 8.1 nm. DT grafting is far harsher: 1DT still retains 244 $m^2\ g^{-1}$, whereas 2DT collapses the structure to 36 $m^2\ g^{-1}$ and 0.06 $cm^3\ g^{-1}$, in agreement with the greatly diminished uptake and narrowed PSD observed in Fig. 5c and d. F-127 is even more sensitive with surface values

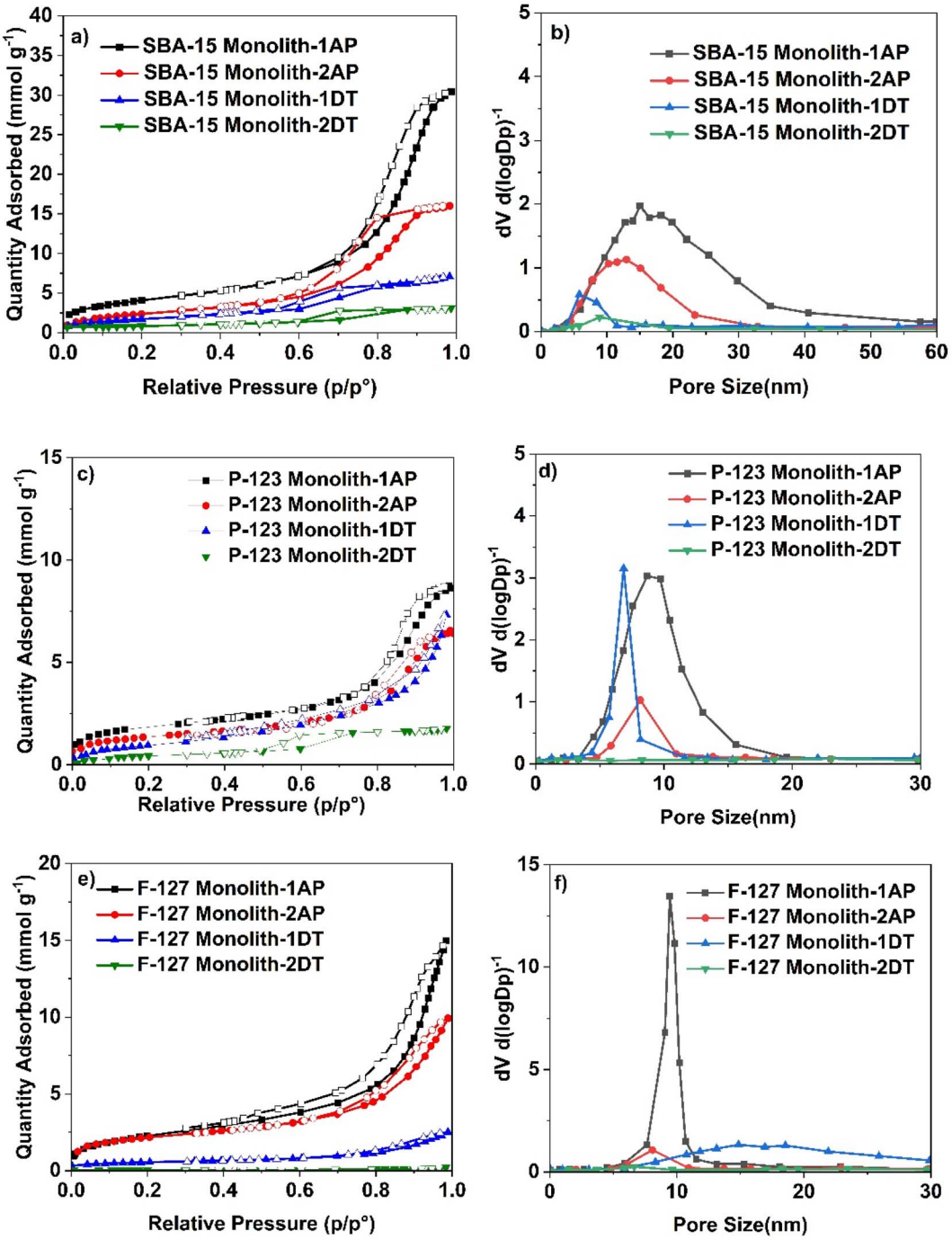

Fig. 5 N_2 adsorption–desorption isotherms at 77 K, and pore size distribution of functionalised (a and b) SBA-15, (c and d) P-123, and, (e and f) F-127 monoliths.

changing from 188 $m^2 g^{-1}$ (1AP) to 147 $m^2 g^{-1}$ (2AP), and 152 $m^2 g^{-1}$ (1DT), but 2DT decreasing to only 3 $m^2 g^{-1}$, signifying almost total pore filling (Fig. 5e and f).

Similar trends were found in the literature. AP grafted samples, both here and in eight analogous studies on silica, KIT6, aerogel and alumina supports,[41,42] show only moderate losses in surface area and pore volume, placing our AP series among the more resilient class II sorbents. In sharp contrast, the F127-2DT specimen undergoes one of the most severe structural contractions yet reported matched only by the rigid APTMS aerogel of Choi *et al.*[43] highlighting the susceptibility of thin-walled Pluronic frameworks at high diamine loadings. SBA15-2DT, despite its high DT content, still retains an open mesopore network (65 $m^2 g^{-1}$, 0.11 $cm^3 g^{-1}$). This underscores the well-known buffering effect of thicker silica walls on structural decay.[40] In general, the change from 1DT to 2DT reflects the well-known "capacity-*versus*-textural properties loss" threshold: when the effective pore diameter approaches twice

Table 2 Textural properties and nitrogen content of functionalised monoliths

Sample	S_{BET} (m^2 g^{-1})	V_p (cm^3 g^{-1})	D_p (nm)	N content (wt%)
SBA-15 monolith	833	1.30	—	—
SBA-15 monolith-1AP	336	1.05	15.1	6.4
SBA-15 monolith-2AP	199	0.55	11.5	7.9
SBA-15 monolith-1DT	145	0.24	5.9	7.4
SBA-15 monolith-2DT	65	0.11	—	10.8
P-123 monolith	435	0.86	11	—
P-123 monolith-1AP	260	0.50	7.8	3.1
P-123 monolith-2AP	149	0.28	8.1	6.0
P-123 monolith-1DT	244	0.76	15.0[a]	7.7
P-123 monolith-2DT	36	0.06	6.0	13.4
F-127 monolith	378	0.75	—	—
F-127 monolith-1AP	188	0.51	8.7	4.6
F-127 monolith-2AP	147	0.28	8.1	6.6
F-127 monolith-1DT	152	0.28	6.9	4.7
F-127 monolith-2DT	3	—	—	6.6

[a] The reported pore diameters (D_p) represent the average pore size estimated using the BJH method. However, some samples, particularly P-123 monolith-1DT, exhibit a broad pore size distribution, indicating the presence of a range of mesopores and macropores rather than a uniform pore structure.

the van-der-Waals span of the oligomeric silane (≈6 nm in P-123 monolith-2DT), multilayer cross-linking blocks access to deeper pores, the same cut-off reported for triamine-grafted alumina honeycombs.[40]

PSD analysis reveals a clear, stepwise progression in structural change. SBA-15 experiences only a modest narrowing of its bimodal meso–macro distribution: even after the 2DT treatment the material still shows a distinct mesopore peak at about 6 nm, a consequence of its wide native channels (15 nm) and thick silica walls. Moving to P-123 monolith, the same high DT loading shifts the principal mesopore peak below 6 nm and partly suppresses the macropore shoulder, pointing to the onset of pore blockage. The effect is most pronounced for F-127 monolith, where 2DT virtually eliminates the mesopore peak, indicating near complete pore filling.

In summary, AP grafting introduces moderate nitrogen loading while largely preserving the mesoporous network. DT grafting yields a much higher amine density but, once a critical loading is exceeded, it leads to pronounced textural collapse. Taken together, the data show that SBA-15 monolith remains the most resilient support, P-123 monolith retains an intermediate level of structural integrity, and F-127 monolith is the most susceptible to collapse, a ranking that reflects the initial textural properties of the three monoliths. Optimizing grafting conditions therefore requires balancing chemical reactivity against the need to maintain accessible porosity.

3.3 CO_2 adsorption studies of functionalised monoliths

The CO_2 adsorption performance of monolithic silica materials before and after functionalisation reveals substantial enhancements attributable to the incorporation of aminosilane groups. As illustrated in Fig. 6 and summarized in Table 3, all functionalised monoliths exhibited notable improvements in CO_2 uptake compared to their non-functionalised counterparts. The SBA-15 monolith functionalised with 2DT displayed a significant uptake of 94 mg CO_2 per g (2.14 mmol of CO_2 per g), substantially outperforming its unfunctionalised version, which achieved 14 mg CO_2 per g. The most pronounced enhancement was observed for the P-123 monolith-2DT, which

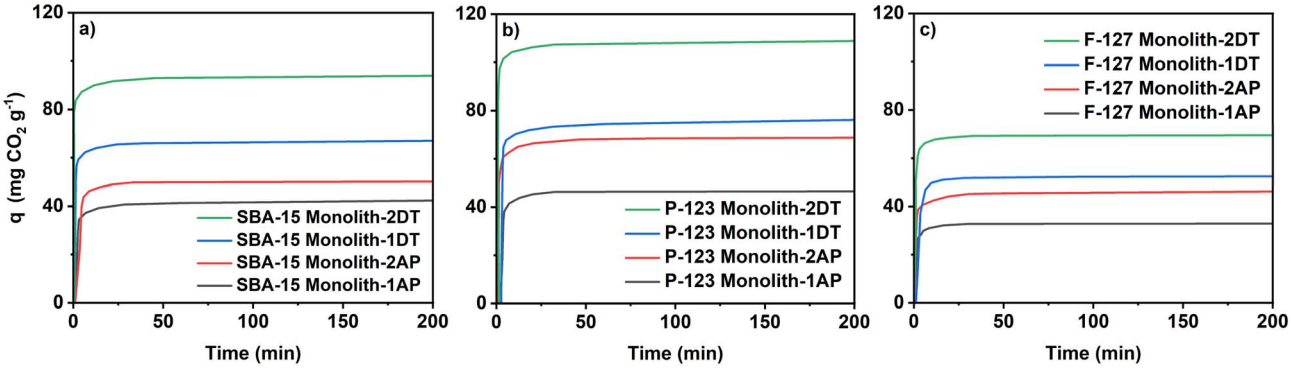

Fig. 6 Pure CO_2 uptake (45 °C, 1 bar) of functionalised monoliths (a) SBA-15, (b) P-123, and (c) F-127 with AP and DT.

Table 3 Nitrogen content and CO_2 adsorption properties of functionalised monoliths

Sample	N content (wt%)	q (mg CO_2 per g)	Amine efficiency[a] (mol of CO_2 per mol of N)
SBA-15 monolith-1AP	6.4	42	0.21
SBA-15 monolith-2AP	7.9	50	0.20
SBA-15 monolith-1DT	7.4	67	0.30
SBA-15 monolith-2DT	10.8	94	0.28
P-123 monolith-1AP	3.1	46	0.47
P-123 monolith-2AP	6.0	69	0.37
P-123 monolith-1DT	7.7	76	0.31
P-123 monolith-2DT	13.4	108	0.26
F-127 monolith-1AP	4.6	33	0.23
F-127 monolith-2AP	6.6	45	0.22
F-127 monolith-1DT	4.7	53	0.36
F-127 monolith-2DT	6.6	70	0.34

[a] Amine efficiency (mol of CO_2 per mol of N) calculated from CO_2 uptake and CHN nitrogen; calculation and uncertainty described in the Experimental section.

exhibited a CO_2 adsorption capacity of 108 mg CO_2 per g (2.45 mmol of CO_2 per g) nearly a tenfold increase relative to the unmodified P-123 monolith (11 mg CO_2 per g). The F-127 monoliths, although exhibiting a lower baseline performance of 6 mg CO_2 per g, also demonstrated increased CO_2 adsorption upon functionalisation, with a maximum uptake of 70 mg CO_2 per g (1.59 mmol of CO_2 per g) in the 2DT sample.

This performance clearly exceeds previously reported amine-grafted silica monoliths. The hierarchically porous APTES monolith of Ko *et al.* adsorbed 1.51 mmol of CO_2 per g at 25 °C,[39] and the 3D-printed aminopropyl contactor of Thakkar *et al.* reached 1.2 mmol of CO_2 per g under comparable conditions.[23] A rigid APTES aerogel prepared by Choi *et al.* exceeds our capacity (3.10 mmol of CO_2 per g)[43] but that material sacrifices roughly 65% of its original porosity, resulting in a high pressure drop. In contrast, the DT-grafted monoliths developed here deliver near-aerogel-level uptake while preserving an integral, low-resistance architecture, underscoring their suitability for practical fixed-bed operation.

These results underscore the pivotal role of surface functionalisation in augmenting the CO_2 capture performance of silica-based monoliths. While the inherent mesoporosity of these materials provides a favourable structural framework, the presence of chemically active sites introduced *via* aminosilane grafting is essential for enhancing CO_2 capacity and affinity. Notably, the rise in CO_2 uptake tracks not only with the total nitrogen introduced but also with how effectively those amine sites remain accessible. This is evident in our own series: although F-127 monolith-2DT reaches the highest nitrogen loading, its almost-blocked pore network delivers a lower molecular efficiency than SBA-15 monolith-2DT, whose wider channels keep the amines available for reaction. The same interplay between amine dispersion and pore accessibility has been demonstrated experimentally for SBA-15, SBA-12 and MCM-41 by Zeleňák *et al.*,[44] where larger pores (SBA-15) supported higher amine surface density and higher CO_2 capacity, whereas narrow MCM-41 pores limited site utilisation despite similar N-content. In line with literature convention, uptake/capacity values taken from previous studies are 1.5 mmol of CO_2 per g. These converging observations confirm that amine distribution and accessibility, rather than nitrogen content alone, govern the overall adsorption performance. This distinction emphasizes the importance of optimizing both the type and concentration of grafted functionalities to balance nitrogen loading with effective site utilisation.

The marked increase in adsorption capacities, particularly with DT-functionalised systems, confirms the viability of this approach in advancing monolithic adsorbents for post-combustion CO_2 mitigation technologies. A comparison with other covalently grafted sorbents is given in Table 4, which confirms that the DT-grafted P-123 monolith sits near the upper end of the performance spectrum for true monolithic contactors.

A relevant indicator of the CO_2 uptake performance is the molar ratio of CO_2 uptake to amine content (mol of CO_2 per mol of N), usually referred to as amine efficiency (listed in Table 3). The AP series shows how capacity and efficiency diverge. P-123 monolith-1AP (3.1% N) adsorbs 46 mg CO_2 per g while presenting a high efficiency of 0.47 mol of CO_2 per mol of N. The use of double AP content in P-123 monolith-2AP (6.0% N) yields smaller efficiency (0.37).

This trend suggests that a higher concentration of AP does not proportionally enhance the utilisation of nitrogen sites, likely due to steric hindrance or reduced accessibility of amine groups, yielding a combination of chemisorption and physisorption processes.[28] At elevated AP loadings, excess amine groups may participate in weaker, non-specific interactions with CO_2 such as physisorption rather than forming strong chemical bonds, thereby reducing the overall efficiency. Previous studies have reported that in amine-functionalised mesoporous silicas,[45] CO_2 is adsorbed *via* both mechanisms: chemisorption at well-dispersed primary amine sites and physisorption at weakly interacting amines or adjacent silanol groups. This dual-mode interaction supports the observed decline in molecular efficiency despite increasing total uptake. Thus, optimizing the amine loading is essential to achieving

Table 4 Equilibrium CO_2 uptakes of covalently amine-grafted sorbents (monoliths, aerogel, powders); comparison with the present work

Material & geometry	Support	CO_2 p (bar)	CO_2 fraction (vol%)	T_{ads} (°C)	N (wt%)	Uptake (mmol of CO_2 per g)	Ref.
1.0 bar, pure CO_2							
HPSM-NH_2 monolith	Hierarchical silica	1	100%	28 °C	5.4[a]	1.51	39
M3-PEI-60 cylindrical monolith	Silica	1	100%	75 °C	18.4[b]	4.16	41
70T-MM-550 gel-cast monolith	MCM-41 silica	1	100%	75 °C	20.0[a]	3.43	28
SBA-15-DT powder	SBA-15 silica	1	100%	45 °C	7.0	1.90	47
P-123-2DT – monolith	P-123 silica	1	100%	45 °C	13.4	2.45	This work
SBA-15-2DT – monolith	SBA-15 silica	1	100%	45 °C	10.8	2.14	This work
F-127-2DT – monolith	F-127 silica	1	100%	45 °C	6.6	1.59	This work
0.15 bar (15% CO_2)							
TA-NH_2-2.5 rigid aerogel	Silica aerogel	0.15	15%	25 °C	8.0	3.10	43
PE-SBA-DT-TEPA powder	Pore-expanded SBA-15	0.15	15%	45 °C	15.3	5.34	46
Other conditions							
PD-TEPA 3-D-printed monolith	Silica	0.1	10%	25 °C	16.1	2.23	23
SA-TRI-1000 honeycomb	γ-Al_2O_3	—	400 ppm	25 °C	9.9	0.46	40

[a] Nitrogen content was calculated based on reported CO_2 uptake (mg CO_2 per g) and amine efficiency (mol of CO_2 per mol of N). [b] Nitrogen content was calculated from the reported PEI content and its molecular structure, assuming 30.7 wt% N.

a balance between adsorption capacity and nitrogen site efficiency in CO_2 capture applications.

The DT series tells a similar story. For example, nitrogen content climbs from 7.7% to 13.4 wt% in DT-functionalised P-123 monolith, pushing CO_2 uptake from 76 mg CO_2 per g to 108 mg CO_2 per g, yet trimming efficiency from 0.31 to 0.26 mol of CO_2 per mol of N.

The overall performance of monolithic adsorbents follows a trend consistent with previous findings, where DT-functionalised monoliths demonstrate superior total CO_2 adsorption capacities compared to their AP-functionalised counterparts. For instance, the P-123 monolith-2DT exhibited the highest CO_2 uptake at 108 mg CO_2 per g, while the analogous AP-functionalised sample, P-123 monolith-2AP, reached a comparatively lower capacity of 69 mg CO_2 per g. Despite the enhanced overall uptake, DT-functionalised materials exhibited a lower molecular efficiency, as evidenced by the lower mol of CO_2 per mol of N ratios. This outcome is attributed to the steric limitations imposed by the bulkier DT molecules, which may hinder the accessibility of nitrogen sites for CO_2 interaction and promote multilayer formation on the silica surface. Such phenomena have been previously documented, indicating that excessive DT loading, while increasing nitrogen content, may compromise the effective utilisation of amine functionalities due to spatial constraints and reduced surface availability.[46]

These findings are consistent with previous reports on amine-grafted mesoporous silicas, where SBA-15 powders functionalised with DT demonstrated enhanced CO_2 adsorption capacities – approximately 1.90 mmol of CO_2 per g at 1 bar and 45 °C – at nitrogen contents around 5.0 mmol of N per g. However, these materials often showed reduced efficiency due to poor utilisation of internal amine groups. On the other hand, SBA-15 samples functionalised with AP, although achieving lower adsorption capacities, exhibited superior molecular efficiency attributed to better accessibility of nitrogen sites.[47]

Fig. 7a and b plot CO_2 uptake and amine efficiency as a function of nitrogen content for all functionalised samples, highlighting the trade-off in adsorption site efficiency commented on above. CO_2 uptake increased almost linearly with

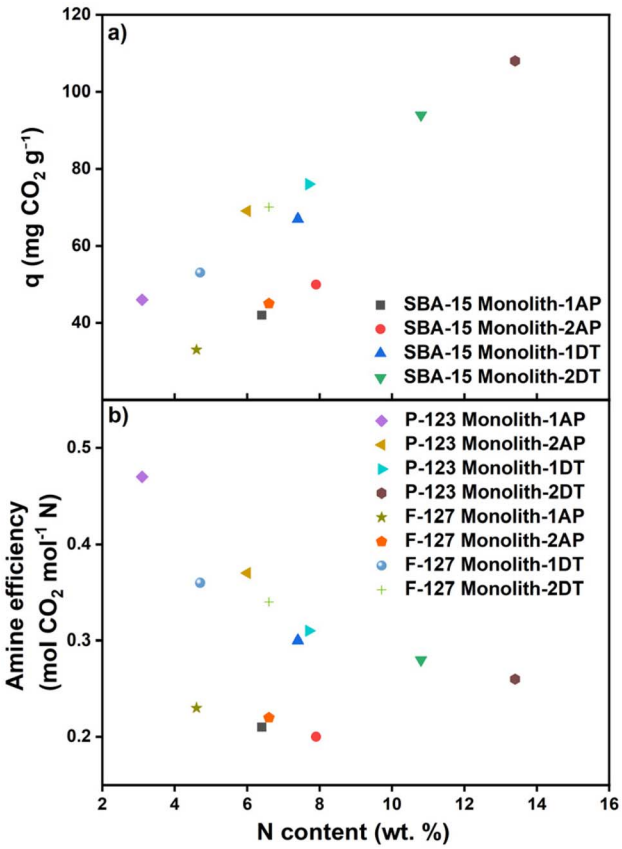

Fig. 7 (a) Adsorption capacity q (mg CO_2 per g) at 45 °C and 1 bar, and (b) amine efficiency (mol of CO_2 per mol of N) *vs.* N content (wt%).

nitrogen loading. However, AP-containing samples, particularly the SBA-15 and F-127 monoliths, displayed lower uptakes than other materials with comparable nitrogen contents. For example, SBA-15 monolith-2AP and P-123 monolith-1DT achieved uptakes of 50 and 76 mg CO_2 per g, respectively, despite having similar nitrogen contents (7.9 and 7.7 wt%).

In contrast, amine efficiency decreased steadily with increasing nitrogen content, consistent with site crowding and diffusional constraints at high loadings. A similar trend was observed for AP-containing samples, which exhibited lower amine efficiencies than their DT counterparts at comparable nitrogen contents. Following the previous example, SBA-15 monolith-2AP and P-123 monolith-1DT reached efficiencies of 0.20 and 0.31 mol of CO_2 per mol of N, respectively, consistent with the different CO_2 uptakes despite comparable nitrogen contents.

Regarding the adsorption mechanism, it is well established that the amino groups of primary and secondary amines react directly with pure CO_2 to form carbamate species.

$$CO_2 + 2RNH_2 \rightarrow RNHCOO^- + RNH_3^+$$

Under dry CO_2, *in situ* DRIFTS analyses of amine-grafted silicas revealed the formation of alkylammonium–carbamate ion pairs along with ammonium entities,[48] while DRIFTS studies using humid CO_2 showed that bicarbonate formation is favoured.[49] Thus, the differences found in the CO_2 adsorption experiments for AP and DT, carried out under pure dry CO_2, having similar nitrogen content, may be attributed to the presence of three amino groups in DT, which increases the likelihood that CO_2 molecules can simultaneously interact with two neighbouring amines, in accordance with the reaction stoichiometry.

Table 4 compares the three samples exhibiting the highest adsorption capacities obtained in the present study, alongside some of the most relevant materials reported in the literature. The monoliths prepared in the present study achieved CO_2 adsorption capacities that are comparable to, or even exceed, those of numerous powdered materials and rigid structures, such as SBA-15-DT powder or HPSM-NH_2 and PD-TEPA 3-D monoliths. The literature materials that surpass the monoliths prepared in the present work are either powdered (PE-SBA-DT-TEPA powder) or have been prepared with much higher amino group contents (M3-PEI-60 cylindrical and 70T-MM-550 gel-cast monolith), some using polymers like polyethyleneimine, PEI, rather than organosilanes such as DT. Another relevant factor is the adsorption temperature. For example, 70T-MM-550 reached a CO_2 uptake of 3.43 mmol of CO_2 per g when analysed at 75 °C, but the value was reduced to 2.43 mmol of CO_2 per g when using a temperature of 50 °C, closer to post-combustion conditions and more in line with the conditions used in the present work (45 °C). Thus, it can be concluded that the materials presented here not only provide a rigid structure, but also possess sufficient porosity to accommodate an adequate amount of amino groups that are also accessible to effectively react with CO_2.

3.4 High-pressure equilibrium CO_2 uptake

The CO_2-adsorption behaviour at higher pressures was determined with a volumetric analyser. Isotherms were recorded in the range 0–6 bar at 45 °C for all AP- and DT-functionalised samples and shown in Fig. 8. All CO_2 isotherms showed a shape typical of chemisorption, with a steep initial uptake at low pressures followed by a plateau, as well as a notable hysteresis upon desorption, suggesting slow or irreversible binding under the adsorption conditions. These features indicate strong interactions between CO_2 molecules and the functionalised surface sites.[18,50]

All isotherms exhibited a significant CO_2 adsorption capacity, which increases with nitrogen content as a result of either a higher organosilane loading or an increased number of amine functionalities per molecule. DT-functionalised SBA-15 monoliths exhibited a substantial enhancement in CO_2 adsorption capacity, with the 2DT-modified sample surpassing 140 mg CO_2 per g at 6 bar. This pronounced increase emphasizes the significant role of elevated nitrogen content in facilitating effective CO_2 retention. The corresponding isotherm reveals a progressive adsorption trend with increasing pressure and minimal desorption at elevated pressures, characteristic of

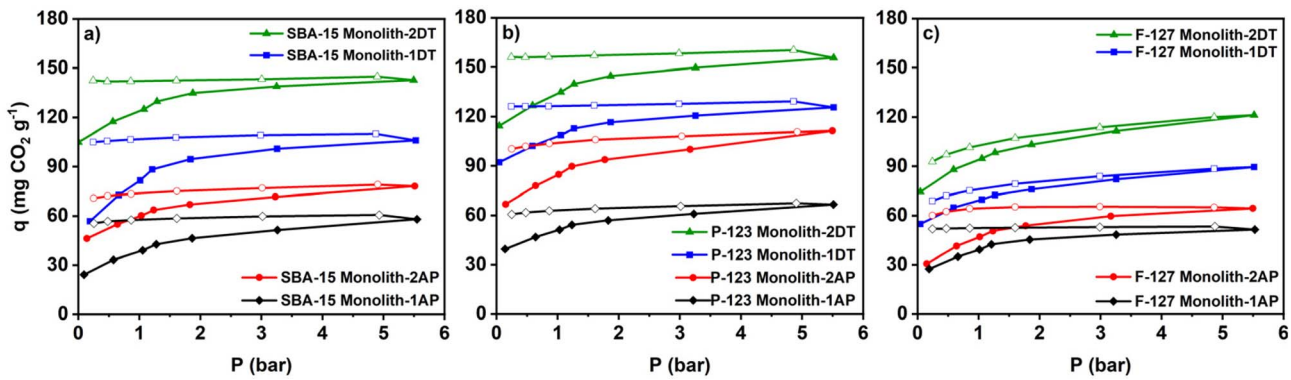

Fig. 8 Pure CO_2 adsorption–desorption isotherms at 45 °C of functionalised monoliths with AP and DT: (a) SBA-15, (b) P-123, and (c) F-127 monoliths.

Table 5 CO_2 uptake of functionalised monoliths at 45 °C (HPVA). Equilibrium uptake at 0.15 bar and ratio to 1 bar

Sample	N (wt%)	HPVA q (mg CO_2 per g) at 0.15 bar	Diluted to pure uptake ratio (%)
SBA-15 monolith-1AP	6.4	25	66%
SBA-15 monolith-2AP	7.9	46	78%
SBA-15 monolith-1DT	7.4	53	65%
SBA-15 monolith-2DT	10.8	108	87%
P-123 monolith-1AP	3.1	38	76%
P-123 monolith-2AP	6.0	65	77%
P-123 monolith-1DT	7.7	94	87%
P-123 monolith-2DT	13.4	116	87%
F-127 monolith-1AP	4.6	21	54%
F-127 monolith-2AP	6.6	31	67%
F-127 monolith-1DT	4.7	56	81%
F-127 monolith-2DT	6.6	77	83%

strong chemisorptive interactions between CO_2 molecules and the amine functionalities introduced *via* DT grafting.

Among the tested samples, the P-123 monolith functionalised with diethylenetriamine (2DT) showed the highest CO_2 uptake, reaching approximately 150 mg CO_2 per g at 6 bar. This represents a substantial improvement compared to the AP-modified analogue (95 mg CO_2 per g) or the one functionalised with a lower amount of DT (120 mg CO_2 per g). This pattern is consistent with earlier reports where CO_2 adsorption capacity was found to be higher for adsorbents containing polyamines like DT due to the higher nitrogen content, although steric crowding could block part of the internal amine sites.[46]

In order to provide a more realistic assessment of CO_2 capture under conditions relevant to flue gas, the CO_2 uptake at low partial pressures (0.15 bar) was estimated from adsorption isotherms. The results are summarized in Table 5, which reports the CO_2 adsorbed at this pressure. To facilitate comparison with uptake under pure CO_2, a "diluted-to-pure uptake ratio" was calculated for each sample. A ratio of 15% would correspond to ideal physical adsorption, where uptake scales proportionally with pressure, whereas a ratio approaching 100% indicates the predominance of chemisorption, reflecting high selectivity towards CO_2 and similar uptake at 0.15 bar and 1.0 bar. The calculated ratios ranged from 54% to 87%, demonstrating that chemisorption significantly contributes to CO_2 capture in all functionalized samples, which exhibit much higher adsorption than would be expected from purely physical interactions. The performance of DT-functionalised samples was again noteworthy, exhibiting ratios between 83% and 87%, confirming their extremely high affinity towards CO_2.

3.5 Cycling stability and performance retention of aminosilane-functionalised monoliths for CO_2 adsorption

A comprehensive evaluation of the cyclic CO_2 adsorption behaviour of monoliths functionalised with aminosilane derivatives-specifically aminopropyl (AP) and diethylenetriamine (DT) – was conducted to assess their stability and performance under repeated adsorption–desorption cycles. The experimental data collected for five adsorption–desorption and regeneration cycles are shown in Fig. 9.

Focusing initially on the AP-functionalised samples, the P-123 monolith-2AP demonstrated notable stability. It began with an initial CO_2 uptake of 69 mg CO_2 per g, showing a modest decrease to 60 mg CO_2 per g by the fifth cycle, thus

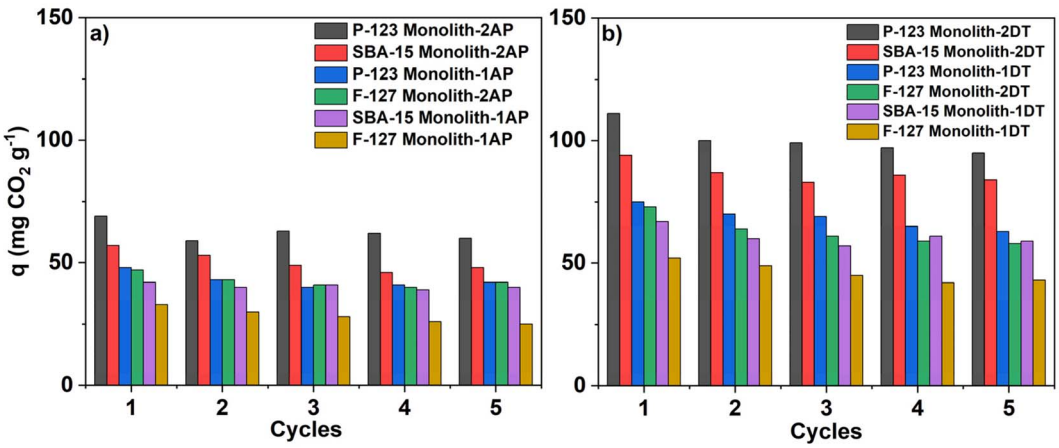

Fig. 9 Cyclic performance of CO_2 adsorption functionalised monoliths with aminosilanes (a) AP and (b) DT.

maintaining 90% of the initial uptake. This limited reduction indicates strong chemical anchoring of the AP groups to the silica framework, suggesting a stable interaction that withstands moderate cyclic thermal stress. Similar trends are observed for SBA-15 and F-127 monoliths modified with AP; although their initial uptake values are comparatively lower, they consistently retain a substantial portion of their original adsorption capacity after repeated cycles, ~96% (SBA-15 monolith-2AP) and ~76% (F-127 monolith-1 AP). These results affirm the suitability of AP-functionalised monoliths for long-term deployment in CO_2 capture applications, where operational consistency and material regeneration are critical factors.[26,43]

DT-functionalised monoliths exhibited a similar durability for multiple adsorption–desorption cycles. For example, the P-123 monolith-2DT initially adsorbs 108 mg CO_2 per g and retains 95 mg CO_2 per g by the fifth cycle, corresponding to 88% of the starting value. This limited decrease also highlights the structural robustness of the DT-functional groups, whose multi-amine configuration likely facilitates strong and persistent interactions with CO_2. Similar stability trends are observed in DT-functionalised SBA-15 and F-127 monoliths, which also maintain high adsorption capacities with minimal degradation across cycles, ranging from 88–89% (SBA-15 monolith) and 81–83% (F-127 monolith).

Further analysis of cycling stability indicates that the most significant reduction in adsorption capacity typically accumulates over the five-cycle duration rather than occurring abruptly in a single cycle. For P-123 monoliths, the 2DT-functionalised sample shows a 12% decline (from 108 mg CO_2 per g to 95 mg CO_2 per g), while the 1DT-functionalised version exhibits a more pronounced 15.8% reduction (from 76 mg CO_2 per g to 64 mg CO_2 per g). AP-functionalised samples display more gradual losses; the P-123 monolith-2AP exhibits a 13% drop (from 69 mg CO_2 per g to 60 mg CO_2 per g), and the P-123 monolith-1AP experiences a minor decrease of 8.7% (from 46 mg CO_2 per g to 42 mg CO_2 per g).

P-123 monolith-2DT was tested over 20 adsorption–desorption cycles under pure CO_2 and a diluted stream of 15% CO_2. Fig. 10 indicates that the stability under pure CO_2 uptake was 85% after 5 cycles and 79% after 20 cycles. This result is consistent with the stability previously observed for 5 cycles, after which the CO_2 uptake appears to approach a plateau. The cyclic test under diluted CO_2 yielded an even higher stability, maintaining 100% of the initial capacity after 5 cycles and 85% after 20 cycles. This supports a longer stability of P-123 monolith-2DT, which makes it suitable for future studies regarding the influence of impurities and/or moisture in the flue gas.

These results demonstrate the feasibility of the engineered monoliths for high efficiency and long-term CO_2 capture, which offer both operational and structural advantages in comparison to powdered adsorbents.[4] It is expected that their organized geometry ensures a lower pressure drop avoiding problems under operational stress, making them well-suited for continuous practical application. Although mechanical testing was not performed here, representative amine-functionalised silica monoliths fabricated by gel-casting based on MCM-41 report axial compressive strengths in the range 4.5–4.7 MPa and radial strengths ≥200 N cm^{-1}, while maintaining high CO_2 capacity.[28] By comparison, formed bodies from other routes span ~0.15–5.5 MPa depending on the formulation and shaping method (*e.g.*, PEI–MSP pellets ~0.50–0.60 MPa; 50% PEI–MCM-41 ~5.5 MPa). These reported ranges indicate that silica-based monoliths can reach handling/packing strength targets typical for packed beds, even at high amine loadings,[24,28] thus pointing to a feasible practical application.

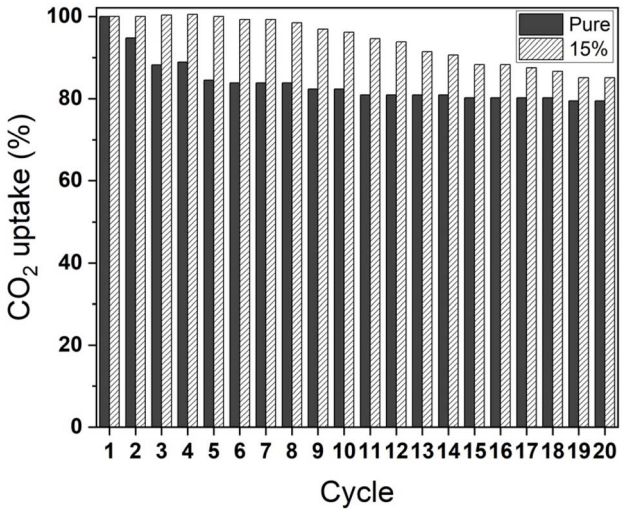

Fig. 10 Cycling stability of CO_2 uptake for P-123 monolith-2DT (45 °C, 1 bar, pure CO_2), normalized to the performance of the first cycle (100%).

4 Conclusion

The findings of this study highlight the critical influence of aminosilane functionalisation in enhancing the CO_2 adsorption performance of Pluronic P-123, F-127, and SBA-15-based monolithic adsorbents. The systematic synthesis of mesoporous silica monoliths and strategic incorporation of organosilanes, specifically 3-(trimethoxysilyl)propylamine (AP) and N^1-(3-trimethoxysilylpropyl)diethylenetriamine (DT), have been instrumental in tailoring the surface chemistry of the monoliths to improve their carbon capture capabilities.

Among the functionalised materials produced, DT-grafting exhibited the most significant improvement in CO_2 adsorption capacity, particularly in the P-123 monolith-2DT sample, which demonstrated both elevated uptake and robust cycling stability. These enhancements are attributed to the multifunctional amine structure of DT, which provides multiple active sites for chemisorption, leading to stronger and stable CO_2 interactions over successive cycles. Such characteristics render DT-functionalised monoliths promising candidates for industrial applications requiring long-term adsorption performance since it displays relevant adsorption capacity, which is maintained over 20 cycles under pure and diluted CO_2 without loss of mechanical integrity. As future work, it will be necessary to

conduct a detailed evaluation of the pressure drop and the mechanical properties of the materials, as well as to assess the influence of impurities and moisture in the feed gas.

Author contributions

Ali Kasiri: methodology, formal analysis, investigation, resources, data curation, writing – original draft, visualization. Raúl Sanz: conceptualization, methodology, writing – review & editing, funding acquisition. Eloy S. Sanz-Pérez: conceptualization, methodology, validation, writing – review & editing, funding acquisition. Amaya Arencibia: conceptualization, methodology, validation, writing – review & editing, funding acquisition.

Conflicts of interest

There are no conflicts to declare.

Data availability

Primary data supporting the description of study are available upon request to the authors of the manuscript.

Acknowledgements

The authors are thankful for the financial support from the Agencia Estatal de Investigación (Ministerio de Ciencia e Innovación, Spain) through the Project TED2021-131144B-I0 and the Community of Madrid and the Rey Juan Carlos University through the Young Researchers R&D Project Ref. M-2177-DESMAT.

References

1 W. M. S. M. Latif, N. M. Sabdullah, S. N. Aenun and N. A. Bosamah, *E3S Web Conf.*, 2024, **516**, 01009.
2 Intergovernmental Panel on Climate Change (IPCC), *Climate Change 2021 – the Physical Science Basis: Working Group I Contribution to the Sixth Assessment Report of the Intergovernmental Panel on Climate Change*, Cambridge University Press, 1st edn, 2023.
3 M. Erans, E. S. Sanz-Pérez, D. P. Hanak, Z. Clulow, D. M. Reiner and G. A. Mutch, *Energy Environ. Sci.*, 2022, **15**, 1360–1405.
4 E. S. Sanz-Pérez, C. R. Murdock, S. A. Didas and C. W. Jones, *Chem. Rev.*, 2016, **116**, 11840–11876.
5 A. A. Abd, S. Z. Naji, A. S. Hashim and M. R. Othman, *J. Environ. Chem. Eng.*, 2020, **8**, 104142.
6 S. Y. Lee and S. J. Park, *J. Ind. Eng. Chem.*, 2015, **23**, 1–11.
7 P. A. Saenz Cavazos, E. Hunter-Sellars, P. Iacomi, S. R. McIntyre, D. Danaci and D. R. Williams, *Front. Energy Res.*, 2023, **11**, 1–22.
8 F. Raganati, F. Miccio and P. Ammendola, *Energy Fuels*, 2021, **35**, 12845–12868.
9 N. Sun, Z. Tang, W. Wei, C. E. Snape and Y. Sun, *Front. Energy Res.*, 2015, **3**, 1–16.
10 U. Farwa, Z. A. Sandhu, A. Kiran, M. A. Raza, S. Ashraf, H. Gulzarab, M. Fiaz, A. Malik and A. G. Al-Sehemi, *RSC Adv.*, 2024, **14**, 37164–37195.
11 S. Mahajan and M. Lahtinen, *J. Environ. Chem. Eng.*, 2022, **10**, 108930.
12 G. L. Seah, L. Wang, L. F. Tan, C. Tipjanrawee, W. A. Sasangka, A. K. Usadi, J. M. McConnachie and K. W. Tan, *ACS Appl. Mater. Interfaces*, 2021, **13**, 36117–36129.
13 S. M. Amaraweera, C. A. Gunathilake, O. H. P. Gunawardene, R. S. Dassanayake, E. B. Cho and Y. Du, *Nanomaterials*, 2023, **13**, 2050.
14 J. Wang, X. Feng, S. Wen, D. Zhan, X. Zhu, P. Ning, Y. Zhang and X. Mei, *Renewable Sustainable Energy Rev.*, 2024, **203**, 114724.
15 E. S. Sanz-Pérez, M. Olivares-Marín, A. Arencibia, R. Sanz, G. Calleja and M. M. Maroto-Valer, *Int. J. Greenhouse Gas Control*, 2013, **17**, 366–375.
16 J. Hack, N. Maeda and D. M. Meier, *ACS Omega*, 2022, **7**, 39520–39530.
17 C. Chen, J. Kim and W. S. Ahn, *Korean J. Chem. Eng.*, 2014, **31**, 1919–1934.
18 S. Bali, J. Leisen, G. S. Foo, C. Sievers and C. W. Jones, *ChemSusChem*, 2014, **7**, 3145–3156.
19 L. Wang and R. T. Yang, *J. Phys. Chem. C*, 2011, **115**, 21264–21272.
20 M. L. Ferreira, M. Pedernera and M. E. Adrover, *Chem. Eng. J.*, 2024, **498**, 155431.
21 X. Li, K. Peng, X. Zhao, K. Zhao, H. Li, Y. Zhao and B. Zhang, *Appl. Clay Sci.*, 2024, **256**, 107433.
22 Y. Wang, J.-T. Anyanwu, Z. Hu and R. T. Yang, *Sep. Purif. Technol.*, 2023, **309**, 123030.
23 H. Thakkar, S. Eastman, A. Al-Mamoori, A. Hajari, A. A. Rownaghi and F. Rezaei, *ACS Appl. Mater. Interfaces*, 2017, **9**, 7489–7498.
24 H. Thakkar, S. Eastman, Q. Al-Naddaf, A. A. Rownaghi and F. Rezaei, *ACS Appl. Mater. Interfaces*, 2017, **9**, 35908–35916.
25 A. Al-Mamoori, A. Krishnamurthy, A. A. Rownaghi and F. Rezaei, *Energy Technol.*, 2017, **5**, 834–849.
26 G. L. Drisko, A. Zelcer, R. A. Caruso and G. J. A. A. Soler-Illia, *Microporous Mesoporous Mater.*, 2012, **148**, 137–144.
27 D. Zhao, J. Feng, Q. Huo, N. Melosh, G. H. Fredrickson, B. F. Chmelka and G. D. Stucky, *Science*, 1998, **279**, 548–552.
28 C. Zhou, S. Yu, K. Ma, B. Liang, S. Tang, C. Liu and H. Yue, *Chem. Eng. J.*, 2021, **413**, 127675.
29 V. Y. Davydov, A. V. Kiselev and L. T. Zhuravlev, *Trans. Faraday Soc.*, 1964, **60**, 2254–2264.
30 L. T. Zhuravlev, *Langmuir*, 1987, **3**, 316–318.
31 M. Thommes, K. Kaneko, A. V. Neimark, J. P. Olivier, F. Rodriguez-Reinoso, J. Rouquerol and K. S. W. Sing, *Pure Appl. Chem.*, 2015, **87**, 1051–1069.
32 E. Shukrun Farrell, Y. Schilt, M. Y. Moshkovitz, Y. Levi-Kalisman, U. Raviv and S. Magdassi, *Nano Lett.*, 2020, **20**, 6598–6605.
33 C. Shi, H. Wang, Q. Bi, L. Li, P. Sun and T. Chen, *ACS Omega*, 2019, **4**, 1443–1448.

34 T. Benamor, L. Vidal, B. Lebeau and C. Marichal, *Microporous Mesoporous Mater.*, 2012, **153**, 100–114.
35 J. Y. Bae, S. G. Jang, J. Cho and M. Kang, *Int. J. Mol. Sci.*, 2025, **26**, 1–27.
36 F. Hoffmann, M. Cornelius, J. Morell and M. Fröba, *Angew. Chem., Int. Ed.*, 2006, **45**, 3216–3251.
37 R. Serna-Guerrero, Y. Belmabkhout and A. Sayari, *Chem. Eng. J.*, 2010, **161**, 173–181.
38 K. S. K. Reddy, A. M. Varghese, A. E. Ogungbenro and G. N. Karanikolos, *ACS Appl. Eng. Mater.*, 2023, **1**, 720–733.
39 Y. G. Ko, H. J. Lee, J. Y. Kim and U. S. Choi, *ACS Appl. Mater. Interfaces*, 2014, **6**, 12988–12996.
40 Q. Grossmann, V. Stampi-Bombelli, A. Yakimov, S. Docherty, C. Copéret and M. Mazzotti, *Ind. Eng. Chem. Res.*, 2023, **62**, 13594–13611.
41 K. Maresz, A. Ciemięga, J. J. Malinowski and J. Mrowiec-Białoń, *Chem. Eng. J.*, 2020, **383**, 123175.
42 J. Babin, J. Iapichella, B. Lefèvre, C. Biolley, J. P. Bellat, F. Fajula and A. Galarneau, *New J. Chem.*, 2007, **31**, 1907–1917.
43 H. Choi, H. H. Han, V. G. Parale, T. Kim, W. Park, Y. Kim, J. Kim, Y. Choi, Y. S. Bae and H. H. Park, *Chem. Eng. J.*, 2024, **483**, 149357.
44 V. Zeleňák, M. Badaničová, D. Halamová, J. Čejka, A. Zukal, N. Murafa and G. Goerigk, *Chem. Eng. J.*, 2008, **144**, 336–342.
45 A. A. Olajire, *Greenhouse Gases:Sci. Technol.*, 2017, **7**, 399–459.
46 R. Sanz, G. Calleja, A. Arencibia and E. S. Sanz-Pérez, *J. Mater. Chem. A*, 2013, **1**, 1956–1962.
47 E. S. Sanz-Pérez, T. C. M. Dantas, A. Arencibia, G. Calleja, A. P. M. A. Guedes, A. S. Araujo and R. Sanz, *Chem. Eng. J.*, 2017, **308**, 1021–1033.
48 A. Danon, P. C. Stair and E. Weitz, *J. Phys. Chem. C*, 2011, **115**, 11540–11549.
49 G. P. Knowles, S. W. Delaney and A. L. Chaffee, *Ind. Eng. Chem. Res.*, 2006, **45**, 2626–2633.
50 A. Samanta, A. Zhao, G. K. H. Shimizu, P. Sarkar and R. Gupta, *Ind. Eng. Chem. Res.*, 2012, **51**, 1438–1463.